Luminol Chemiluminescence Catalyzed by Silver Nanoparticles for the Sensitive Determination of Penicillamine

Fakhr Eldin O. Suliman* and Kauther Al-Hadhrami

Department of Chemistry, College of Science, Sultan Qaboos University, Box 36, Al-Khod 123, Sultanate of Oman. *Email: fsuliman@squ.edu.om.

ABSTRACT: A sequential injection method for the determination of penicillamine (PA) was developed based on quenching the chemiluminescence generated by oxidation of luminol by hydrogen peroxide in presence of silver nanoparticles (AgNPs). The chemiluminescence (CL) of the reaction was found to greatly enhance in presence of AgNPs due to the increased catalyst surface area. The method was sensitive and found suitable for analysis of penicillamine in pharmaceutical preparations. Linear calibration curve is obtained in the range 0.2-1.0 μg mL^{-1} with a relative standard deviation less than 2%. A recovery percent of 102.3 $\pm$0.2 was obtained with the tablets matrix indicating reasonable selectivity of the method for PA in tablets. The mechanism of quenching of the CL reaction was investigated by UV-Visible spectroscopy and transmission electron microscopy as well as by theoretical calculations using DFT-B3LYP method. The covalent attachment of PA to the AgNPs triggers aggregation of the particles thereby diminishing the surface significantly. The method was applied for the assay of PA in pharmaceutical preparations.

Keywords: Chemiluminescence; Silver nanoparticles; Sequential injection analysis; Pharmaceutical preparations and Penicillamine.

وميض الليمونيل الكيميائي بواسطة جسيمات النانوـ فضة كعامل مساعد لتحليل البنسالامين

فخر الدين سليمان و كوثر الحضرمي

الملخص: تم إستحداث طريقة حقن إنسيابي لتحليل البنسالامين بواسطة تثبيط التضوءالكيميائي الناشئ عن تفاعل الليمونول مع بيروكسيد الهيدروجين في وجود جسيمات الفضة النانوية. التضوء الناتج عن تفاعل الليمونول يزداد بصورة كبيرة في وجود الجسيمات النانوية. الطريقة المستحدثة ذات حساسية عالية وتم تطبيقها على تحليل البنسالامين في المستحضرات الصيدلانية. وجد منحنى المعايرة بين 200-1000 نانوجرام/مل كما أن الانحراف المعياري النسبي لم يزد عن 2%. بالإضافة لذلك ما تم استرجاعه من البنسالامين عند تحليله في منتجاته الصيدلانية كان 0.2 ± 102.3% وهذا يدل على أن الطريقة المستحدثة مناسبة لتحليل هذا الدواء في المنتجات الصيدلانية. تم أيضًا في هذا البحث دراسة الآلية التي يتم بها تثبيط تضوء الليمونول بواسطة البنسلامين وذلك بإستخدام طرق عملية وأخرى نظرية.

الكلمات المفتاحية: التضوءالكيميائى ، جسيمات الفضة النانوية ، حقن إنسيابي، مستحضرات صيدلانية و بنسالامين.

1. Introduction

An intense interest has been lately directed towards the design, synthesis and application of nanostructures. Myriads of articles have appeared in the literature describing the wide variety of applications of these fascinating materials in analytical, biomedical, optical, electrical and magnetic fields [1–9]. The major attraction to these materials is due to the size and shape dependent optical, catalytic and electro-magnetic properties [10]. NPs of narrow size distribution can be produced when all nuclei are formed at the same time; from these nuclei or seeds other nanostructures of uniform sizes can be developed.

Silver and gold nanoparticles have been considered as hallmark during exploitation of Surface Enhanced Raman Spectroscopy, a technique that opened new avenues in research allowing detection of agrochemicals, biochemical molecules and toxins at ultra-trace levels and making it an important diagnostic technology [11–17]. Moreover, silver is known for its high toxicity to a wide range of microorganisms, this has, in turn, driven lots of attention to investigate AgNPs as a promising antimicrobial agent [18,19].

In many instances the surface chemistry of the NPs influences their interaction with the other systems, such as microorganisms. Capping agents such as citrates are used to stabilize the particles in solution; however, the physicochemical properties of the ensuing NPs depends greatly on the nature of these agents [10].

The chemiluminescence of luminol was known since the first half of the previous century. Luminol CL is produced by oxidizing the reagent with strong oxidizing agents such as hydrogen peroxide and usually in the presence of a catalyst. Metal ions such as Co(II), Cu(II) and Ag(I) have been extensively used as catalysts. AgNPs were found to catalyze this CL reaction producing intense emission possibly due to the high electron density imparted by the high surface area of the small particles [3,20,21]. Other metal nanoparticles such as AuNPs, Au/Ag alloy NPs and PtNPs also enhance the CL of luminol in presence of various oxidants [20–23]. However, AgNPs exhibit the highest catalytic activity which has been rationalized by the lower reduction potential of Ag compared to Au and Pt [10]. The smooth oxidation of Ag produces an abundant population of hydroxyl radicals on the surface of particles and consequently intense CL is obtained.

Enhancement and quenching of luminol-H_2O_2-metal-NPs CL has been used as a platform for developing a number of analytical methods for the determination of various pharmaceutical and biomedical species. For example, sensitive methods for determination of fluoroquinolones, glutathione, and the anticancer drug flutamide were developed based on their enhancement effects on the luminol-metal-NPs CL [6, 20, 21, 23–24]. On the other hand, quenching of this CL reaction by N-acetyl-cysteine enabled determining low levels of this drug in pharmaceutical preparation [25].

Voicescu *et al.* evaluated the antioxidant activity of hydroxyflavones in presence of bovine and human serum albumin using luminol-H_2O_2-AgNPs CL [26]. A method for ultrasensitive determination of DNA hybridization has been developed based on luminol-AgNPs CL [27]. In this method the high sensitivity of the CL together with the large number of Ag ions allowed specific sequence DNA targets to be detected.

The major advantages of CL have led to the extensive utilization of this technique for detection of analytes using flow injection analysis, sequential injection analysis, microfluidics, capillary electrophoresis and high performance liquid chromatography[28–35]. The major attraction to CL detection in these techniques stems from the high sensitivity and the simple instrumentation as only a photomultiplier tube is required, eliminating the use of expensive optics required by other techniques such as fluorescence spectroscopy. In CL the absence of an external light source does not only eliminate the need for use of monochromator but also reduces background signals and scattering generated by other species or by walls of cuvettes.

Penicillamine (PA), (2-Amino-3-mercapto-3-methyl-butyric acid), Figure 1, is a sulfhydryl molecule with a chemical structure similar to the amino acid cysteine. It is a metabolite of the antibiotic penicillin, but with no antibiotic properties. Currently PA is used to treat some disorders such as Wilson's disease and cystinuria [36,37]. PA treatment hinges on its binding ability of accumulated heavy elements such as copper with ensuing elimination through urination.
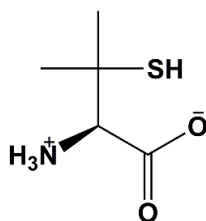

Figure 1. Chemical structure of penicillamine.

Inspired by the above reports, the effect of PA on the CL of luminol-H_2O_2-AgNPs was investigated. We also investigated the relationship between the size and shape of AgNPs and the CL intensity. An analytical method was further based on the quenching effect of PA on luminol-H_2O_2-AgNPs CL and was developed using sequential injection analysis (SIA) together with CL detection for the analysis of PA in pharmaceutical preparations. It is worth mentioning here that, SI-technique is characterized by its low consumption of reagents compared to the pristine flow injection analysis. Moreover, we investigated the mechanism of CL quenching by PA using experimental methods and theoretical calculations.

2. Experimental

2.1 General

All reagents were used without further purification. Tri-sodium citrate (>99%), sodium borohydrate ($NaBH_4$) and hydrated hydrazine were obtained from BDH Chemicals (Pool, England). $AgNO_3$, NaOH, 30% (w/w) H_2O_2, penicillamine 99% and luminol (97%) were from Aldrich (USA). Penicillamine film coated tablets BP was from Genenic (UK). Ultra-pure water from a Milli-Q system was used for all solution preparation and experiments.

Transmission electron microscope (JEOL JEM-1230) was used for the determination of particle size and shape. Absorption spectra were recorded on CARY 50 Conc. spectrophotometer (Varian). A SLM Amnico Bowman series-2 luminescence spectrometer was used to record emission spectra as well as to collect chemiluminescence (CL)

emissions by optimizing the photomultiplier tube (PMT) voltage from 850-1000 V and by keeping the excitation slit closed. The flow-through cell for CL was fabricated from a Teflon transparent tubing of 0.75 mm id. The tube is coiled in a circular pattern of 3 cm diameter and attached to a mirror to capture the maximum light intensity and placed just in front of the PMT. AB2 software was used to control all processes of the luminescence spectrometer.

2.2 Synthesis of silver nanoparticles

Citrate-protected silver seeds were prepared as follows: 0.5 mL of 59 mmol L^{-1} $AgNO_3$ and 1 mL of 34 mmol L^{-1} sodium citrate were added to 98 mL of deionized water. The solution was stirred for 15 minutes and 0.5 mL of aqueous 0.02 mol L^{-1} $NaBH_4$ solution, which had been stored for 2 h, was added dropwise. The resulting olive solution was stirred vigorously for 1 hour and stored for 1 day in the dark at room temperature before use. Silver seeds were approximately spherical with average diameter of 12 nm from transmission electron microscopy (TEM) measurements. Silver nanoparticles, AgNPs, of various sizes and shapes were obtained starting with the seed prepared. Different volumes of silver seeds (15-5 mL) were added to a solution containing 300 μL hydrazine (40 mmol L^{-1}) and 100 μL sodium citrate (40 mmol L^{-1}). To this solution 100 μL of an aqueous solution of 59 mmol L^{-1} silver nitrate were added dropwise with vigorous stirring. The growth of the particles resulted in four different nanostructures (A1-A4).

For TEM analysis, 1 mL of each sample (A1–A4) was centrifuged for purification and the solid portion was washed twice with deionized water. All samples were placed in ultra-sonic machine to homogenize nanoparticles for 15 min before the preparation of the TEM grids. A drop of sample was placed on wax film and the formvar/carbon film (300 mesh Cu grid) was placed on the top of the drop for 30 to 60 seconds. Grids were lifted from the drop with care and dried with clean filter paper and stored after that in grid box for scanning.

2.3 Preparation of solutions

A 10 mmol L^{-1} stock solution of luminol was prepared by dissolving 443 mg luminol powder in 250 mL 0.02 mol L^{-1} NaOH solution. Working solutions of 0.8 mol L^{-1} H_2O_2 were prepared daily from 30% (w/w) H_2O_2.

A stock solution of 1000 μg mL^{-1} of PA was prepared by dissolving 10 mg of the drug into 10 mL volumetric flask filled to the mark with deionized water. Working solutions of PA were prepared by appropriate dilution.

A stock solution of PA tablets was prepared by crushing six PA tablets after weighing each tablet. An amount of powder that correspond to a average tablet mass (78 mg) of PA was dissolved in 50.0 mL water. The solution was sonicated for one hour and then filtered and stored in cold for further use. Working solutions of PA were prepared by appropriate dilutions of the filtered stock solution.

2.4 Manifold and procedure

The sequential injection analysis system used in this study is schematized in Figure 2. It consists of 5.0 mL syringe pump driven by a stepper motor (24000-step full stroke), 200 cm holding coil (0.8 mm ID Teflon tubing, Upchurch Scientific, Oak Harber, USA), a multiposition-valve (eight ports, Valco, Houston, USA), 100 cm and 20 cm reaction coils (0.8 mm ID Teflon tubing, Upchurch Scientific). A second 1.0 mL syringe pump was used to drive the reagent H_2O_2 through the flow system. A homemade flow cell of a 3.0 cm diameter (0.8 mm ID Teflon tubing, Upchurch Scientific) attached to a mirror to maximize collection of emitted light was placed in front of the detector. All fluids were controlled by FIAlab for windows software.
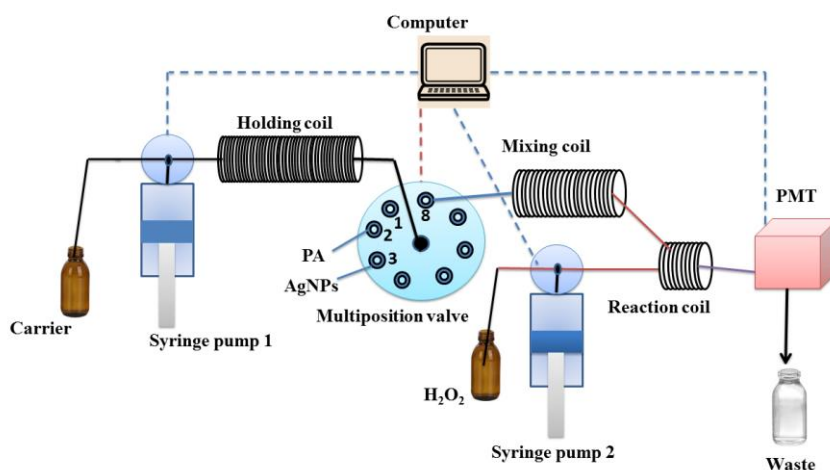

Figure 2. SIA manifold used for the analysis of PA with luminol-H_2O_2-AgNPs CL system.

CL signals were obtained by aspirating the reagent luminol and standard solution of penicillamine with Ag-NPs into holding coil by multiposition-valve and the composite zone was then pumped by syringe pump 1 towards the detector. The second syringe pump, syringe pump 2, was synchronized to pump appropriate volumes of the oxidant H_2O_2 to meet the composite zone of luminol-PA-AgNPs at T-junction just before the reaction coil, then the mixture was passed to the flow cell and the CL emission produced was collected and measured by PMT.

2.5 Molecular modeling

The geometry of PA, PA-Ag complex, and their dimers were optimized using the density functional theory (DFT) calculations in conjunction with the B3LYP gradient-corrected hybrid [38,39]. The 6-31G(d) basis set was selected for all atoms except silver for which LANL2DZ effective core potential was used [40]. The final geometry was confirmed as a true minimum by inspecting the harmonic vibrational frequencies showing no imaginary frequencies. All calculations were performed using Gaussian 09 software.

3. Results and Discussion

3.1 Synthesis and characterization of AgNPs

AgNPs were prepared at room temperature using a mixture of silver nitrate, sodium citrate, and $NaBH_4$ in aqueous solution. The solution mixture turned light yellow immediately and changed to olive color upon stirring for one hour. This signals the formation of AgNPs. Strong reducing agents favors the formation of smaller nanocrystals due to the fast rate of reaction [10,41]. Further, AgNPs of different sizes and shapes were obtained by controlling the number of seeds in the solution. In this work we used milder reducing agents, hydrazine and citrate ions, the latter works as a capping agent as well. In presence of silver seed further reduction of silver ions results in particle growth which was inferred from a noticeable change of color of the solution. Because of the catalytic effect of silver seed secondary nucleation of AgNPs is prohibited which leads to growth of particles [41,42].

Figure 3 shows a typical TEM image of Ag-nanostructures. These nanostructures are of different shapes and sizes. The almost spherical particles are characterized by a size range of 4.0-20 nm in diameter. This wide range of particle size is associated with the rapid nucleation which characterizes precipitations from solutions.

Figure 4A shows the UV-Visible absorption spectrum of AgNPs. The maximum absorption was at 395 nm, which is due to the presence of AgNPs with an average diameter of 12 nm. Figure 4B shows the absorption spectra of the solution of the AgNPs (samples A1-A4). The prepared solutions show a visible change of color from yellow through greenish blue to red, while for A4 it was cyan. The location of peaks is closely correlated with the size of the AgNPs and nanoplates. The higher the size of the NPs and nanoplates, the further the location of this peak extends toward the near IR region. The peak around 400 nm was due to spherical silver particles, which are caused by incomplete seeding growth in two dimensions and the percent of these spherical silver particles is few because the absorption intensity of the peak is quite weak. The origin of the peak at 338 – 360 nm was not known at present but it could be due to complexes of silver in the solution.
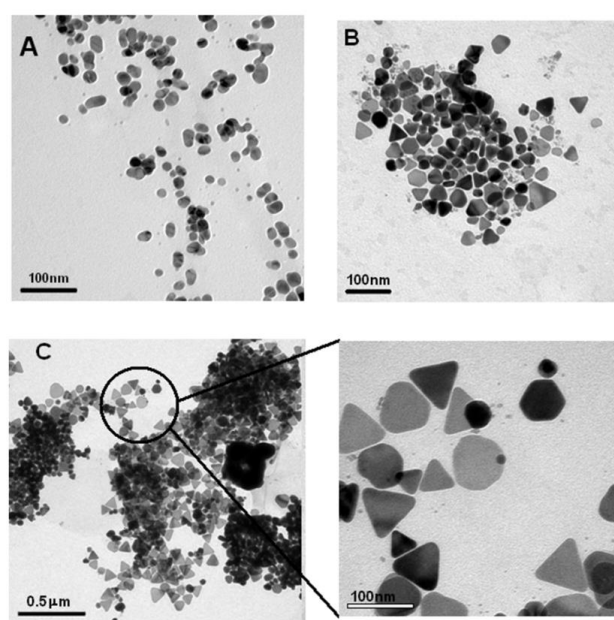

Figure 3. TEM images of (A) silver nanoparticles; (B) and (C) are nanoplates for sample A2 and sample A3 respectively through step-by-step growing.

3.2 AgNPs-luminol-H_2O_2 CL

Luminol-H_2O_2 CL system is a popular CL system and as Figure 5 shows it emits weak CL in alkaline solution in the absence of a catalyst. In this work the catalytic effect of AgNPs on the luminol-H_2O_2 CL system was investigated. When AgNPs were added into the system, the signal remarkably enhances. Interestingly, adding Ag-nanoplates enhance s the CL signal of luminol- H_2O_2 sytem as well but to a lesser extent compared to AgNPs. This is due to large catalytic area provided by AgNPs compared to the nanoplates. We therefore, investigated the AgNPs-luminol- H_2O_2 system to develop an analytical protocol for the determination of PA.
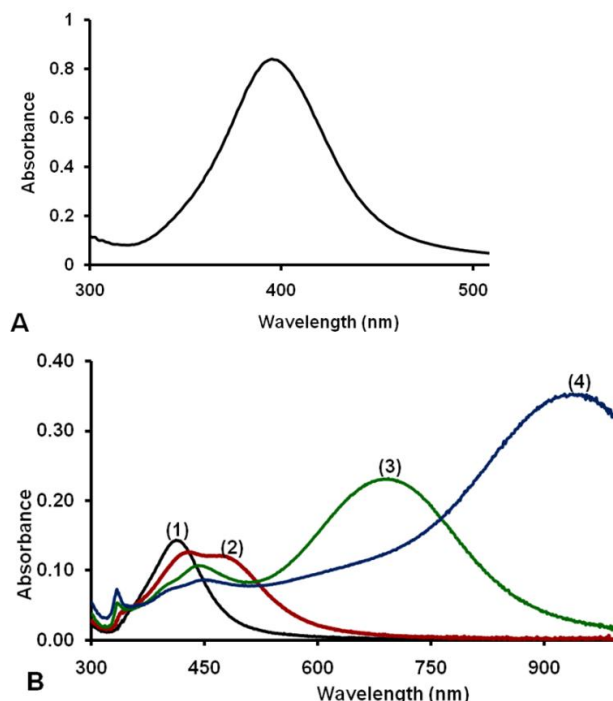

Figure 4. UV-Vis-NIR spectra of prepared AgNPs and nanoplate solutions: (A) AgNPs, and (B) samples A1-A4 respectively: (1) sample A1; (2) sample A2; (3) sample A3; (4) sample A4.

3.3 Optimization

The experimental factors that affect the enhancement of luminol-H_2O_2 CL by AgNPs included in this work are given in Table 1. The effect of each of these factors was examined by the univariate approach where each factor was changed while keeping other factors constant.

The effect of the concentration of NaOH solution on the CL system was studied from 0.010 M - 0.10 mol L^{-1}. It is well documented that oxidation of luminol by H_2O_2 takes place in alkaline media. The intensity of CL emission was observed to increase with NaOH concentration until it reaches 0.020 mol L^{-1} and then it started to decrease. Therefore the NaOH concentration was fixed at 0.020 mol L^{-1}.

The effect of H_2O_2 concentration on the CL was also studied in the range of 0.10 - 1.5 mol L^{-1}. The CL intensity increases as the concentration of H_2O_2 increases up to 0.80 mol L^{-1}, after which the signal intensity remains virtually constant with further increase in H_2O_2 concentration. Therefore, the optimum concentration of H_2O_2 was selected to be 0.80 mol L^{-1}.

Table 1. Factors included in the optimization study and their optimum.

Factors	Range	Optimum
Size of Ag-NPs	(Ag-NPs) – (Ag-nanoplates)	AgNPs
NaOH concentration	0.010 M – 0.10 mol L^{-1}	0.020 mol L^{-1}
H_2O_2 concentration	0.10 M - 1.5 mol L^{-1}	0.80 mol L^{-1}
Ag-NPs conc.	1mL in 10 mL H_2O – not diluted	4 mL in 10 mL H_2O

CL intensity was also found to increase as the concentration of the nanoparticles increases. The increase of catalytic area was the major reason for this phenomenon, because as the concentration of the nanoparticles increases, the available catalytic area increases as well and the detectable CL intensity enhances significantly. Notably, the CL signal increases exponentially with an increase in the amount of AgNPs. The enhancement factor upon addition of the maximum amount of AgNPs (8 mL of as-prepared AgNPs) was about 300 times compared to CL emissions in the

absence of nanoparticles. However, for further experiments only 4 mL of the as-prepared AgNPs will be used as a compromise between sensitivity and cost. The optimum conditions for AgNPs-luminol-H_2O_2 are summarized in Table 1. These conditions will be used for the determination of PA.

3.4 Analysis of PA

A typical sequential injection (SI) results are shown in Figure 5 for the quenching effect of PA on the CL of AgNPs-luminol- H_2O_2 system. The luminol-H_2O_2 system in absence of AgNPs emits weak CL signal. Addition of AgNPs increases the intensity of the signal significantly. Interestingly, addition of PA results in a noticeable quenching of the CL emission especially in presence of AgNPs.
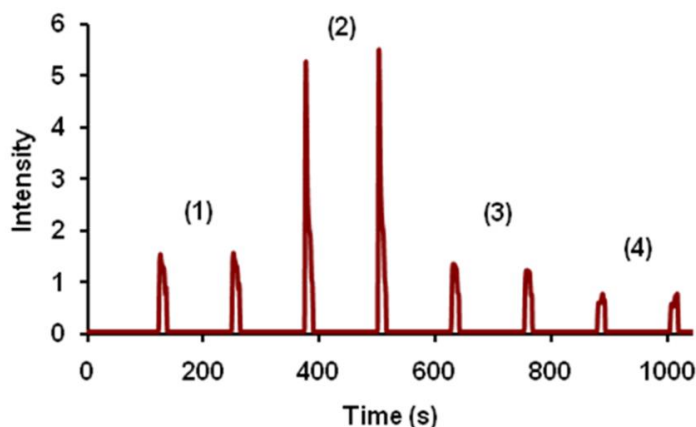

Figure 5. Typical SI results of (1) Luminol-H_2O_2, (2) Luminol-H_2O_2- Ag-NPs, (3) Luminol-H_2O_2- Ag-NPs- PA, (4) Luminol - H_2O_2 - PA.

These results suggest that AgNPs-luminol-H_2O_2 can be used to develop an analytical procedure for the assay of PA in pharmaceutical forms based on quenching of this reaction. Series of SI runs were obtained by injecting standard solution of PA in the range 200-1000 ng mL^{-1} in presence of constant amount of AgNPs. Mixing of these solutions with luminol and H_2O_2 generated the signals shown in Figure 6. Obviously, this figure shows a gradual decrease in CL with increasing concentrations of PA and as can be seen highly reproducible results are always obtained. This is an advantage of utilizing the SI technique, where each run is affected in the same way as other runs. Each standard was run in duplicate and each run was repeated three times and a relative standard deviation less 2% is obtained at all times. Regression analysis of I_0/I versus concentration of PA, $C_{PA}(\mu g\ mL^{-1})$, produced the following calibration equation: $I_0/I = 7.8\pm0.4\ C_{PA} + 0.7\pm0.2\ (R^2 =0.99)$.
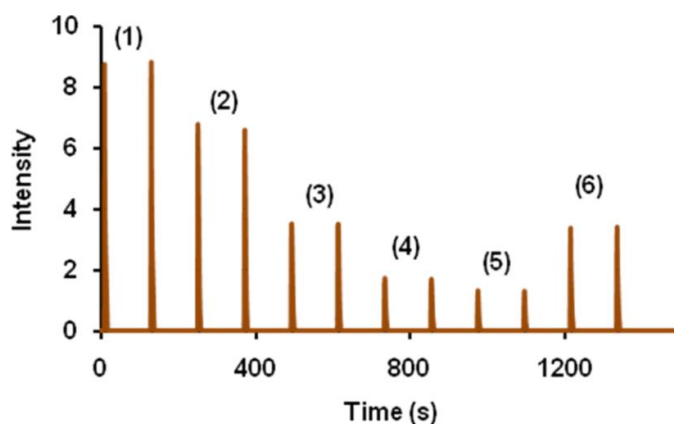

Figure 6. Typical SI results of standard PA and PA sample produced using optimum conditions shown in Table 1: (1) no PA; (2) 0.20 μg mL^{-1} PA; (3) 0.40 μg mL^{-1} PA; (4) 0.60 μg mL^{-1} PA; (5) 0.80 μg mL^{-1} PA; (6) 0.40 μg mL^{-1} PA tablets (drug sample).

The proposed method was applied for the determination of PA in pharmaceutical formulations of commercial dosage forms. Tablets were prepared as described before. From the SI results of standards PA of different concentrations and 0.40 μg mL^{-1} PA tablets solution, it was noticed that the prepared tablet solution of PA has the same effect as standard solution of same concentration (Figure 6). The recovery for this sample was calculated to be 102.3 ± 2.2% indicating that no interference is observed from the additives present in the tablets.

3.5 CL quenching mechanism

Metal cations such as Co(II) are known to catalyze the decomposition of hydrogen peroxide to produce the reactive hydroxyl radicals and the superoxide species ($^\bullet$O$_2$) [43,44]. The high surface area of AgNPs is, therefore, responsible for the efficacy of production of large bursts of highly reactive radicals. It is also widely accepted that NPs surface contribute to the creation of luminol radical intermediates. The radical-radical annihilation reaction of luminol with hydroxyl or superoxide species generates a blue CL emission. Thiols such as PA possess a number of functional groups that might interact with AgNPs as well as with the catalytically generated species. Therefore, PA is expected to compete with luminol to intermediate hydroxyl and superoxide radicals resulting in quenching of the CL intensity. Moreover, the formation of Ag-S covalent bond might result in covering AgNPs surface with PA molecules and subsequently decreases the catalytic activity of the particle surface.

To investigate the mechanism of quenching of luminol-H$_2$O$_2$- Ag-NPs system by PA, series of solutions containing constant amount of luminol, H$_2$O$_2$, AgNPs and varying concentrations of PA (0.0 – 5.0 μg mL^{-1}) were prepared. The SI-CL signals for these solutions show that as the concentration of PA is increased the CL signal decreases sharply and the signal was observed to decrease more than fifty times by adding 5 μg mL^{-1} of PA.

UV-Visible spectra of AgNPs in absence and presence of increasing amount of PA were obtained. An absorption peak was observed between 392 and 398 nm for all different concentration of PA with a change in color of the solution from dark yellow to light pink with the addition of high PA concentration. It was also observed that the absorbance decreased with an increase in PA concentration. Moreover, it was observed that at high concentration of PA absorption spectra started to shift to higher wavelength and became broader.

To further investigate the effect of the addition of PA to the luminol - H$_2$O$_2$ - AgNPs system, TEM images (before and after the addition of PA) were taken as shown in Figure 7. The TEM images show that prior to addition of PA, the particles are highly dispersed and approximately of uniform size in aqueous solution with an average diameter of 12 nm. After the addition of PA, the AgNPs became highly aggregated and connected. It is worth mentioning here that these samples were prepared by centrifuging the mixture, separating the nanoparticles and washing with deionized water twice.

The above observations can be explained as follows: the addition of PA to a solution containing AgNPs results in the covering the surface of AgNPs with PA through the sulfur group of PA and the surface Ag atoms of the nanoparticles. This in turn leads to the aggregation of AgNPs due to the formation of strong hydrogen bonding between the different functional groups (carboxyl and amine groups) on the surface. This leads to the reduction of the catalytic activity of Ag-NPs and as a result the CL intensity of luminol decreases.
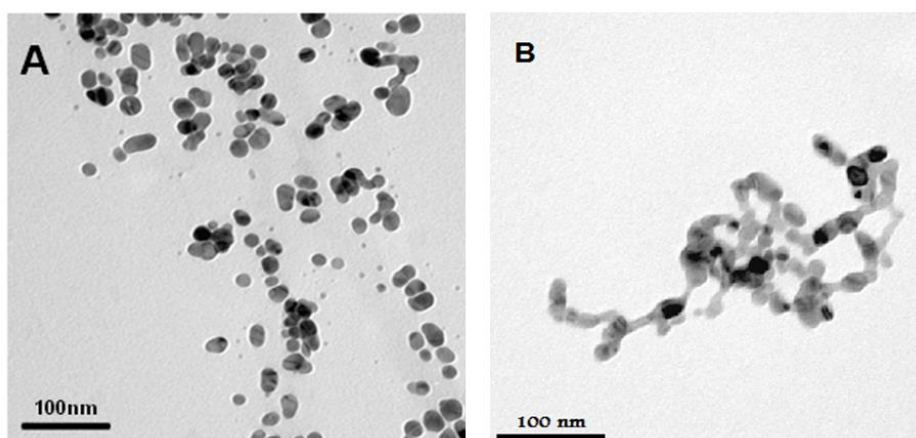

Figure 7. TEM and photograph images of 4 nm – 25 nm Ag-NPs: (A) before and (B) after the addition of PA.

We also performed theoretical calculations to study the possible intermolecular interaction between PA molecules attached to Ag ions. The geometries of PA and its corresponding Ag complex are obtained by DFT calculations and the optimized geometry of PA-Ag complex is shown in Figure 8. The calculated Ag-S bond distance is 2.398 Å and the Ag-S-C bond angle is 105.7°. Moreover, the calculated dihedral angles NCCO in the complex and in the free molecule were 159.4° and 163.1° respectively. This indicates that amine and the carbonyl conserves the same planarity when complexed to silver; similar results were reported for N-acetyl-L-cysteine with silver [45]. The

optimized structure of Ag-PA-PA-Ag dimer is also shown in Figure 8. These dimers are formed by interaction of PA molecules with one another. Inspection of this figure reveals the fact that the presence of the amino and the carboxyl groups facilitated the formation of a network of strong intermolecular hydrogen bonds. This network of hydrogen bonding is established through the interaction of the hydrogen atoms on the amine groups with the oxygen atoms on the carboxyl group. The hydrogen bond lengths between the hydrogen atoms on the amine group and the two oxygen atoms of the carboxyl group are 1.735 and 1.627 Å. This in turn results in aggregation of nanoparticles and consequently the CL intensity is quenched.
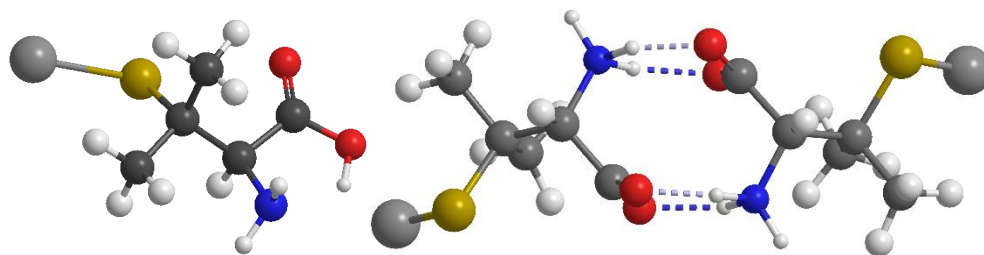

Figure 8. DFT-B3LYP Optimized structures of (a) PA-Ag (b) Ag-PA-PA-Ag.

4. Conclusion

In this work we successfully prepared silver nanostructures of different sizes and shapes. AgNPs of spherical shape with average diameter of 12 nm were found to efficiently catalyze luminol-H_2O_2 reaction to produce an intense CL. PA quenched effectively the CL emission and based on this quenching effect an analytical procedure was developed for the analysis of PA in pharmaceutical samples. The mechanism of quenching was investigated using experimental and theoretical methods. It was found that quenching of the CL is due to agglomeration of AgNPs driven by the hydrogen bonding interactions between PA molecules attached to silver ions on the surface of AgNPs.

References

1. Han, S., Liu, B., Liu, Y. and Fan, Z. Silver nanoparticle induced chemiluminescence of the hexacyanoferrate-fluorescein system, and its application to the determination of catechol. *Microchimica Acta,* 2016, **183**, 917–921.
2. Xu, S.-L. L. and Cui, H. Luminol chemiluminescence catalysed by colloidal platinum nanoparticles. *Luminescence*, 2007, **22**, 77–87.
3. Iranifam, M., Imani-Nabiyyi, A., Khataee, A. and Kalantari, J. Enhanced luminol–O $_2$ chemiluminescence reaction by CuO nanoparticles as oxidase mimics and its application for determination of ceftazidime. *Analytical Methods*, 2016, **8**, 3816–3823.
4. Ji, X., Wang, W., Li, X., Chen, Y. and Ding, C. Enhanced chemiluminescence detection of glutathione based on isoluminol-PSM nanoparticles probe. *Talanta*, 2016, 2016, **150**, 666–670.
5. Chaichi, M.J., Alijanpour, S.O., Asghari, S. and Shadlou, S. Evaluation of luminol chemiluminescence based on simultaneous introducing of coumarin derivatives as green fluorophores and chitosan-induced Au/Ag alloy nanoparticle as catalyst for the sensitive determination of glucose. *Journal of Fluorescence,* 2015, **25**.
6. Liu, W., Guo, Y., Li, H., Zhao, M., Lai, Z. and Li, B. A paper-based chemiluminescence device for the determination of ofloxacin. *Spectrochimica Acta - Part A Molecular and Biomolecular Spectroscopy,* 2015, **137**, 1298–1303 .
7. Wang, S., Wu, Q., Wang, H., Zheng, X., Shen, S., Zhang, Y., Miao, J. and Zhao, B. Biosensors and Bioelectronics Novel pyrazoline-based fluorescent probe for detecting glutathione and its application in cells. *Biosensensors Bioelectronics,* 2014, **55**, 386–390.
8. Safavi, A., Absalan, G. and Bamdad, F. Effect of gold nanoparticle as a novel nanocatalyst on luminol-hydrazine chemiluminescence system and its analytical application. *Analytica Chimica Acta,* 2008, **610**, 243–248.
9. Bae, D.R. *et al.* Lysine-functionalized silver nanoparticles for visual detection and separation of histidine and histidine-tagged proteins. *Langmuir*, 2010, **26**, 2181–2185.
10. Guo, J.Z., Cui, H., Zhou, W. and Wang, W. Ag nanoparticle-catalyzed chemiluminescent reaction between luminol and hydrogen peroxide. *Journal of Photochemistry and Photobiology: A Chemistry*, 2008, **193**, 89–96 .
11. Feng, S., Hu, Y., Ma, L. and Lu, X. Development of molecularly imprinted polymers-surface-enhanced Raman spectroscopy/colorimetric dual sensor for determination of chlorpyrifos in apple juice. *Sensors and Actuators, B Chemical,* 2017, **241**, 750–757.
12. Tite, T., Ollier, N., Sow, M.C., Vocanson, F. and Goutaland, F. Ag nanoparticles in soda-lime glass grown by continuous wave laser irradiation as an efficient SERS platform for pesticides detection. *Sensors and Actuators, B Chemical,* 2017, **242**, 127–131.
13. Zheng, J., Zhao, C., Tian, G. and He, L. Rapid screening for ricin toxin on letter papers using surface enhanced Raman spectroscopy. *Talanta*, 2017, **162**, 552–557.

14. Chen, Y., Zhang, Y., Pan, F., Liu, J., Wang, K., Zhang, C., Cheng, S., Lu, L.-G., Zhang, Z., Zhi, X., Zhang, Q., Zhang, W., Chen, D., Alfranca, G., De La Fuente J.M. and Cui, D. Breath analysis based on surface enhanced raman scattering sensors distinguishes early and advanced gastric cancer patients from healthy persons. *ACS Nano*, 2016,**10**, 8169–8179.

15. Xiao, R., Zhang, X., Rong, Z., Xiu, B., Yang, X., Wang, C., Hao, W., Zhang, Q., Liu, Z., Duan, C., Zhao, K., Guo, X., Fan,Y., Zhao, Y., Johnson, H., Huang, Y., Feng, X., Xu, X., Zhang, H. and Wang, S. Non-invasive detection of hepatocellular carcinoma serum metabolic profile through surface-enhanced Raman spectroscopy. *Nanomedicine Nanotechnology, Biology and Meicine*, 2016, **12**, 2475–2484.

16. Cao, X., Shi, Lu, C.W., Zhao, H., Wang, M., Zhang, M., Chen, X., Dong, J., Han, X. and Qian, W. Surface enhanced Raman scattering probes based on antibody conjugated Au nanostars for distinguishing lung cancer cells from normal cells. *Journal of Nanoscience and Nanotechnology,* 2016, **16**, 12161–12171.

17. Birtoiu, I.A., Rizea, C., Togoe, D., Munteanu, R.M., Micsa, C., Rusu, M.I., Tautan, M., Braic, L., Scoicaru, L.O., Parau, A., Becherescu-Barbu, N.D., Udrea, M.V., Tonetto, A., Notonier, R. and Grigorescu,C.E.A., Diagnosing clean margins through Raman spectroscopy in human and animal mammary tumour surgery: A short review. *Interface Focus*, 2016, **6**.

18. Elechiguerra, J.L., Burt, J.L., Morones, J.R., Camacho-Bragado, A., Gao, X., Lara, H.H. and Yacaman, M.J. Interaction of silver nanoparticles with HIV-1. *Journal of Nanobiotechnology* , 2005, **3**, 6.

19. Cao, G. and Wang, Y. "*Nanostructures and Nanomaterials: Synthesis, Properties and Applications"*. World Scientific Publishing Co., Singapore, 2011.

20. Zhang, Z.F., Cui, H., Lai, C.Z. and Liu, L.J. Gold nanoparticle-catalyzed luminol chemiluminescence and its analytical applications. *Analytical Chemistry*, 2005, **77**, 3324–3329.

21. Wang, L. *et al.* A flow injection chemiluminescence method for the determination of fluoroquinolone derivative using the reaction of luminol and hydrogen peroxide catalyzed by gold nanoparticles. *Talanta*, 2007, **72,** 1066–1072 .

22. Kamruzzaman, M., Alam, A.-M., Lee, S. H.H. and Dang, T.D.D. Chemiluminescence microfluidic system on a chip to determine vitamin B1 using platinum nanoparticles triggered luminol-$AgNO_3$ reaction. *Sensors and Actuators, B Chemical,* 2013, **185**, 301–308.

23. Chaichi, M.J.M.J., Azizi, S.N.S.N. and Heidarpour, M. A novel luminol chemiluminescent method catalyzed by silver/gold alloy nanoparticles for determination of anticancer drug flutamide. *Spectrochimica Acta - Part A Molecular and Biomolecular Spectroscopy*, 2013, **116**, 594–598.

24. Wabaidur, S. mohammad, Alam, S.M., Alothman, Z.A. and Mohsin, K. Silver nanoparticles enhanced flow injection chemiluminescence determination of gatifloxacin in pharmaceutical formulation and spiked urine sample. *Spectrochimica - Acta Part A Molecular Biomolecular Spectroscopy,* 2015, **144**, 170–175.

25. Samadi-Maybodi, A. and Akhoondi, R. Trace analysis of N-acetyl-L-cysteine using luminol-H_2O_2 chemiluminescence system catalyzed by silver nanoparticles. *Luminescence*, 2015, **30**, 775–779.

26. Voicescu, M., Nistor, C.L.C.L. and Meghea, A. Insights into the antioxidant activity of some flavones on silver nanoparticles using the chemiluminescence method. *Journal of Luminsence,* 2015, **157**, 243–248.

27. Liu, C.-H., Li, Z.-P., Du, B.-A., Duan, X.-R. and Wang Y.-C. Silver nanoparticle-based ultrasensitive chemiluminescent detection of DNA hybridization and single-nucleotide polymorphisms. *Analytical Chemistry,* 2006, **78**, 3738–3744.

28. Kamruzzaman, M., Alam, A.-M., Kim, K.M., Lee, S.H., Kim, Y.H., Kabir, A.N.H., G.-M. Kim. and Dang, T.D. Chemiluminescence microfluidic system of gold nanoparticles enhanced luminol-silver nitrate for the determination of vitamin B12. *Biomedical Microdevices*, 2013, **15**, 195–202.

29. Al Lawati, H.A.J., Kadavilpparampu, A.M. and Suliman, F.O. Combination of capillary micellar liquid chromatography with on-chip microfluidic chemiluminescence detection for direct analysis of buspirone in human plasma. *Talanta*, 2014, **127**, 230–238.

30. Ge, L., Wang, S., Ge, S., Yu, J., Yan, M., Li, N. and Huang, J., Electrophoretic separation in a microfluidic paper-based analytical device with an on-column wireless electrogenerated chemiluminescence detector. *Chemical Communications* 2014, **50**, 5699–5702.

31. Chen, X. *et al.* Determination of beta-agonists in swine hair by μFIA and chemiluminescence. *Electrophoresis*, 2015, **36**, 986–993.

32. Kadavilpparampu, A.M., Al-Lawati, H.A. J., Suliman, F.O. and Al Kindy, S.M.Z. Determination of the pseudoephedrine content in pharmaceutical formulations and in biological fluids using a microbore HPLC system interfaced to a microfluidic chemiluminescence detector. *Luminescence*, 2015, **30**, 1242–1249.

33. Al Haddabi, B., Al Lawati, H.A.J. and Suliman, F.O. An enhanced cerium(IV)-rhodamine 6G chemiluminescence system using guest-host interactions in a lab-on-a-chip platform for estimating the total phenolic content in food samples. *Talanta*, 2016, **150**, 399–406.

34. Wang, H., Li, Zhang, J.X., Hu, B., Liu, Y., Zhang, L., Cha, R., Sun, J. and Jiang, X. A microfluidic indirect competitive immunoassay for multiple and sensitive detection of testosterone in serum and urine. *Analyst*, 2016, **141**, 815–819.

35. Al Haddabi, B., Al Lawati, H.A.J. and Suliman, F.O. A comprehensive evaluation of three microfluidic chemiluminescence methods for the determination of the total phenolic contents in fruit juices. *Food Chemistry,*

2017, **214**, 670–677.

36. Walshe, J. M. The story of penicillamine: A difficult birth. *Movement Disorders*, 2003,**18**, 853–859.

37. Derk, C.T., Huaman, G. and Jimenez, S.A. A retrospective randomly selected cohort study of D-penicillamine treatment in rapidly progressive diffuse cutaneous systemic sclerosis of recent onset. *British Journal of Dermatology,* 2008, **158**, 1063–1068.

38. Becke, A.D. Density-functional thermochemistry. III. The role of exact exchange. *Journal of Chemical Physics,* 1993, **98**, 5648–5652.

39. Lee, C., Yang, W. and Parr, R.G. Development of the Colle-Salvetti correlation-energy formula into a functional of the electron density. *Physics Review B*, 1988, **37**, 785–789.

40. Hay, P.J. and Wadt, W.R. Ab initio effective core potentials for molecular calculations. Potentials for K to Au including the outermost core orbitale. *Journal of Chem. Physics,* 1985, **82**, 299–310.

41. Qi, H., Alexson, D., Glembocki, O. and Prokes, S.M. The effect of size and size distribution on the oxidation kinetics and plasmonics of nanoscale Ag particles. *Nanotechnology* , 2010, **21**, 215706.

42. Jana, N.R., Gearheart, L. and Murphy, C.J. Seeding growth for size control of 5-40 nm diameter gold nanoparticles. *Langmuir*, 2001, **17**, 6782–6786.

43. Liu, Y.-M., Liu, E.-B. and Cheng, J.-K. Ultrasensitive chemiluminescence detection of sub-fM level Co(II) in capillary electrophoresis. *Journal of Chromatography. A*, 2001, **939**, 91–97.

44. Wheatley, R.A., Sariahmetoglu, M. and Cakici, I. Enhancement of luminol chemiluminescence by cysteine and glutathione. *Analyst*, 2000, **125**, 1902–1904.

45. Abbehausen, C., Heinrich, T.A., Abrão, E.P., Costa-neto, C.M., Lustri, W.R., Formiga, A.L.B. and Corbi, P.P. Chemical , spectroscopic characterization , DFT studies and initial pharmacological assays of a silver(I) complex with N-acetyl-L-cysteine. *Polyhedron*, 2011, **30**, 579–583.